NASA TECHNICAL NOTE

NASA TN D-7520

NASA TN D-7520

BOUNDARY-LAYER ANALYSIS OF SUBSONIC INLET DIFFUSER GEOMETRIES FOR ENGINE NACELLES

by James A. Albers and E. John Felderman

Lewis Research Center

Cleveland, Ohio 44135

NATIONAL AERONAUTICS AND SPACE ADMINISTRATION • WASHINGTON, D. C. • MARCH 1974

1. Report No. NASA TN D-7520	2. Government Accession No.	3. Recipient's Catalog No.
4. Title and Subtitle BOUNDARY-LAYER ANALYSIS OF SUBSONIC INLET DIFFUSER GEOMETRIES FOR ENGINE NACELLES		5. Report Date MARCH 1974
		6. Performing Organization Code
7. Author(s) James A. Albers and E. John Felderman		8. Performing Organization Report No. E-7816
9. Performing Organization Name and Address Lewis Research Center National Aeronautics and Space Administration Cleveland, Ohio 44135		10. Work Unit No. 501-24
		11. Contract or Grant No.
12. Sponsoring Agency Name and Address National Aeronautics and Space Administration Washington, D.C. 20546		13. Type of Report and Period Covered Technical Note
		14. Sponsoring Agency Code

15. Supplementary Notes

16. Abstract

Theoretical Mach number distributions and boundary-layer parameters are presented for subsonic nacelle inlet diffuser geometries with length to exit diameter ratios ranging from 0.4 to 1.6 and diffuser exit area to throat area ratios ranging from 1.1 to 2.0. The major portion of the study was done with a cubic diffuser contour with the inflection point at the midpoint of the diffuser, a diffuser throat Mach number of 0.6, and a free-stream Mach number of 0.12. Calculations were performed at both model (diffuser exit diameter, 30.5 cm) and full-scale (diffuser exit diameter, 183 cm) sizes. Separation limits were defined by establishing a separation boundary on plots of diffuser area ratio as a function of diffuser length to diameter ratio. The effects of diffuser contour, inlet lip geometry, and throat Mach number on the boundary-layer characteristics are illustrated. The major results of the study indicate that the separation boundary is shifted to greater area ratios by (1) increasing the diffuser length, (2) increasing the scale of the diffuser and, (3) moving the inflection point of the diffuser contour to or ahead of the midpoint of the diffuser.

17. Key Words (Suggested by Author(s)) Boundary layer separation; Diffuser; Inlet flow; Engine nacelle; Induction system; Boundary layer flow	18. Distribution Statement Unclassified - unlimited Cat. 12

19. Security Classif. (of this report) Unclassified	20. Security Classif. (of this page) Unclassified	21. No. of Pages 30	22. Price* $3.00

* For sale by the National Technical Information Service, Springfield, Virginia 22151

BOUNDARY-LAYER ANALYSIS OF SUBSONIC INLET DIFFUSER GEOMETRIES FOR ENGINE NACELLES

by James A. Albers and E. John Felderman*

Lewis Research Center

SUMMARY

Theoretical Mach number distributions and boundary-layer parameters are presented for subsonic nacelle inlet diffuser geometries with length to exit diameter ratios ranging from 0.4 to 1.6 and diffuser exit area to throat area ratios ranging from 1.1 to 2.0. The major portion of the study was done with a cubic diffuser contour with the inflection point at the midpoint of the diffuser, a diffuser throat Mach number of 0.6, and a free-stream Mach number of 0.12. Calculations were performed at both model (diffuser exit diameter, 30.5 cm) and full-scale (diffuser exit diameter, 183 cm) sizes. Separation limits were defined by establishing a separation boundary on plots of diffuser area ratio as a function of diffuser length to diameter ratio. The effects of diffuser contour, inlet lip geometry, and throat Mach number on the boundary-layer characteristics are illustrated. The major results of the study indicate that the separation boundary is shifted to greater area ratios by (1) increasing the diffuser length, (2) increasing the scale of the diffuser, and (3) moving the inflection point of the diffuser contour to or ahead of the midpoint of the diffuser.

INTRODUCTION

A continuing problem in the development of aircraft engine nacelles is the design of efficient subsonic inlet diffusers which provide high total pressure recovery, low total pressure distortion, and uniform flow to the engine compressor during low-speed and cruise operation. In general, the designer tries to avoid flow separation on the diffuser surface to enhance the compatibility between the inlet and engine. Most of the diffuser design guidelines presently available are empirical and are based on correlations of

*Assistant Professor of Mechanical Engineering, South Dakota State University, Brookings, South Dakota; NASA Summer Faculty Fellow at Lewis Research Center in 1973.

experimental data (e.g., ref. 1). Diffuser performance maps based on empirical correlations have been published by Reneau (ref. 2) for incompressible two-dimensional flow and by Sovran (ref. 3) for incompressible annular flow. More recent experimental work in diffusers can be found in references 4 and 5. The design of inlet diffusers for engine nacelles requires more information than generally appears on diffuser performance maps (such as entrance Mach number and entrance boundary-layer displacement thickness) since nacelle inlet geometry and engine performance must also be considered. Thus, there is a definite need to establish design guidelines for the selection of separation-free diffuser geometries for engine inlets.

Design guidelines were obtained by using a calculation procedure (ref. 6) to determine the potential flow and two-dimensional boundary-layer characteristics of axisymmetric inlet diffuser geometries in a compressible viscous flow for a wide range of flow conditions. Comparisons of the potential flow theory with experimental data for inlets are given in references 7, 8, and 9. An application of the potential flow calculation procedure to investigate subsonic inlet lip geometries is given in reference 10. Experimental data for boundary-layer comparisons for inlet diffusers are not available. However, a comparison of boundary-layer theory with experimental data for other applications is given in references 11 and 12.

This report presents the results of an analytical study to investigate the boundary-layer characteristics of inlet diffuser geometries for turbofan engines. The purpose of the study is to establish general guidelines for the selection of a separation-free diffuser geometry. To obtain realistic boundary-layer conditions at the diffuser entrance a complete inlet configuration including lip and external forebody is used. The inlet diffuser geometric variables investigated are diffuser length to diameter ratio (0.4 to 1.6), diffuser area ratio (1.1 to 2.0), and diffuser contour. The effect of inlet lip geometry on the diffuser boundary-layer characteristics is also presented. Boundary-layer displacement thicknesses, shape factors, and skin friction coefficients are presented for both model and full-scale sizes. Separation boundaries are also established at various flow conditions.

The major emphasis of this study is on the low-speed (takeoff and landing) operating conditions. For all low-speed conditions the free-stream Mach number is 0.12 with inlet incidence angles of 0° and 40°. The effects of throat Mach number (ranging from 0.5 to 0.8) were also investigated.

SYMBOLS

A flow area

C_f skin friction coefficient

D diameter

H shape factor, ratio of displacement thickness to momentum thickness

L length

M Mach number

V velocity

X surface distance from diffuser entrance plane

α inlet incidence angle, angle between free-stream velocity and inlet axis

β maximum wall angle

δ^* displacement thickness

$\theta/2$ equivalent conical half angle

Subscripts:

c centerbody

d diffuser

e exit

max maximum

T cowl throat

1 highlight

∞ free stream

ANALYSIS

Definition of Diffuser Geometries

The principal geometric variables for the inlet diffuser are illustrated in figure 1. To ensure realistic boundary-layer conditions at the start of the diffuser entrance, a complete inlet geometry including inlet lip and external forebody was used for this investigation. The diffuser was taken to start at the point of the inlet throat (X = 0, fig. 1). The geometries are representative of conventional subsonic inlets with an NACA series one external cowl shape and a two-to-one ellipse internal lip. The internal lip area contraction ratio A_1/A_T $\left(D_1^2/D_T^2\right)$ is 1.35 for the major portion of the study. The inlet maximum diameter to diffuser exit diameter was kept constant at $D_{max}/D_e = 1.11$. For this investigation all the diffusers included a centerbody. The centerbody diameter to diffuser exit diameter was constant at $D_c/D_e = 0.4$. The centerbody length to diffuser exit diameter was also constant at $L_c/D_e = 0.4$. The centerbody contour was a two-to-one ellipse.

The inlet diffuser geometric variables investigated are diffuser length to diameter ratio L_d/D_e, diffuser area ratio A_e/A_T, and diffuser contour. The diffuser length to diameter ratio varied from 0.4 to 1.6 with diffuser area ratios ranging from 1.1 to 2.0. This range covers most subsonic inlet diffusers for engines. Figure 2 illustrates each diffuser investigated with their associated geometry identification number. The actual values of all geometric variables used in this study are given in table I. The equivalent conical half angle $\theta/2$ shown in table I is defined as

$$\frac{\theta}{2} = \arctan\left(\frac{\sqrt{\frac{A_e}{\pi}} - \sqrt{\frac{A_T}{\pi}}}{L_d}\right)$$

The diffuser contour for the major portion of the study was a cubic, which has an inflection point at the midpoint of the diffuser length. An illustration of the diffuser geometries with cubic contours are shown in figure 3. Diffusers 17 and 18 of table I are the same as the cubic contour of diffuser 10 with different lip contraction ratios. Besides the cubic, other contours were generated which have inflection points located at 25 and 75 percent of the length of the diffuser (fig. 4). The inflection points were located on the conical diffuser line, that is, on a straight line drawn from the diffuser entrance to the diffuser exit. The contours were generated by using two superellipse curves (ref. 13) and by keeping the slope at the midpoint and endpoint of the diffuser for all three contours approximately the same.

Calculation Procedure

The inlet potential and viscous flows were obtained by using four computer programs (fig. 5). The first program, SCIRCL (ref. 13), establishes the coordinates and point spacing on the inlet surfaces. Program EOD is the Douglas axisymmetric incompressible potential flow program. The method is discussed in detail in reference 14. It is used to obtain three basic solutions for flow about inlets which are used as the input to a third computer program called COMBYN. The method of this program is described in detail in reference 15. It combines the basic solutions to obtain a solution for any combination of free-stream velocity, inlet incidence angle, and mass flow rate through the inlet. COMBYN also corrects the incompressible potential flow solution for compressibility using the method described in reference 16. The surface Mach number distributions obtained from COMBYN were used as input to VISCUS, which calculates the boundary-layer growth and separation point (if any) on the inlet surface. VISCUS (ref. 17) is a modified version of the Herring and Mellor program (ref. 11), which calculates the laminar and turbulent boundary-layer development in compressible flow. The location of the transition region from laminar to turbulent flow in VISCUS was determined from empirical correlations of reference 18. For more details of the calculation procedure see references 6 and 17.

The boundary-layer growth was calculated on the cowl surface from the stagnation point on the inlet lip to the diffuser exit. The Falkner-Skan laminar wedge flow solution for stagnation point flow was used for a starting profile. In calculating the boundary-layer parameters, the surface was assumed to be smooth and the free-stream turbulence was assumed to be zero. The effects of surface shocks and longitudinal curvature were neglected. The longitudinal curvature enters the boundary-layer analysis as a correction term in the turbulent viscosity hypothesis (ref. 11). The criterion used to determine the point of separation is the condition of zero wall shear stress (zero skin friction coefficient).

The boundary-layer calculations were made two-dimensional, since relatively small differences existed between two-dimensional and axisymmetric calculations. In general, for the diffuser geometries considered, the boundary-layer thicknesses were thin relative to the changes in surface radii. The boundary-layer thickness is slightly thinner for axisymmetric calculations than for two-dimensional calculations. Thus, the results contained in this report would be slightly conservative (i.e., the diffuser geometries with axisymmetric calculations would be less likely to separate). Circumferential flows in the boundary layer were neglected. The effect of secondary flows may be important for inlet diffuser geometries at angle of attack.

DISCUSSION OF RESULTS

The effects of diffuser area ratio A_e/A_T and diffuser length to diameter ratio L_d/D_e on the diffuser boundary-layer characteristics are first discussed with a fixed diffuser contour and throat Mach number. This is followed by a discussion of the effect of diffuser contour, inlet lip geometry, and throat Mach number.

Effect of Diffuser Area Ratio and Diffuser Length to Diameter Ratio

For this portion of the study, geometries 1 to 12 of figure 3 are investigated. The diffuser contour is a cubic with the inflection point at the midpoint of the diffuser length, and the one-dimensional throat Mach number M_T is 0.6. Both model (D_e = 30.5 cm) and full-scale (D_e = 183 cm) sizes are considered at low-speed conditions at zero angle of attack. Also, the results for model size at angle of attack and cruise conditions will be discussed.

Low-speed conditions at zero angle of attack. - Potential flow and boundary-layer calculations were obtained for a free-stream Mach number M_∞ of 0.12, an inlet incidence angle α at 0^o, and at a model size D_e of 30.5 centimeter (1 ft). Surface Mach number distributions and boundary-layer parameters are presented in figure 6 for four of the shorter diffusers (L_d/D_e from 0.4 to 0.8) and in figure 7 for four of the longer diffusers (L_d/D_e from 0.8 to 1.6). The figures are plotted against the nondimensional surface distance from the diffuser entrance X/D_e. The Mach number distributions (part (a) of figs. 6 and 7) are also shown for negative values of X/D_e since the stagnation point occurs ahead of the diffuser entrance. The boundary-layer parameters presented are skin friction coefficient C_f (part (b)), nondimensional displacement thickness δ^*/D_e (part (c)), and shape factor H (part (d)).

A close examination of Mach number distributions indicates the overall Mach number gradient in the diffuser increases with diffuser area ratio A_e/A_T and decreases with length to diameter ratio L_d/D_e. For example, for a constant L_d/D_e of 0.4 (diffusers 1 and 2, fig. 6(a)), the overall Mach number gradient increases as A_e/A_T is increased. For a constant A_e/A_T (diffusers 6 and 11, fig. 7(a)), the overall Mach number gradient decreases as L_d/D_e increases. Thus, a conservative diffuser would be long with a low area ratio. However, a general design objective is to design the shortest diffuser (to minimize weight and skin friction losses) whose surface is separation free. Guidelines for determining the optimum length and area ratio can be obtained by examining the boundary-layer parameters for the various geometries.

The results of figures 6(b) and 7(b) show that the flow of diffusers 2, 3, and 6 are separated while the flow of diffusers 1, 5, 8, 10, and 11 are not separated. The skin friction coefficient C_f drops rapidly in the diffuser and becomes zero when separation occurs. For attached flow conditions, the skin friction coefficient reaches a minimum nonzero value which occurs in the region of minimum Mach number gradient. The minimum value of skin friction coefficient can be used as a measure of the proximity to separation.

The displacement thickness (figs. 6(c) and 7(c)) increases at a faster rate for the geometries where separation is observed and reaches its maximum value at the separation location. For the nonseparated flow conditions, the displacement thickness reaches a maximum value in a region of the minimum local Mach number gradient and then decreases near the diffuser exit where small favorable Mach number gradients occur. The fall off of the boundary-layer displacement thickness can be attributed to both the local Mach number gradients and the sensitivity of the displacement thickness to the local boundary-layer velocity profile.

The shape factor (figs. 6(d) and 7(d)) decreases downstream of the diffuser entrance ($X/D_e = 0$) and reaches a minimum value in the 1.6 to 1.8 range. Transition to turbulent flow was predicted just downstream of the diffuser entrance. As the flow decelerates the shape factor increases. If separation occurs, the shape factor exceeds a value of 2.2.

If separation does not occur, H reaches a maximum value in the region of minimum skin friction coefficient and then decreases as the Mach number gradient becomes small.

To summarize the previous results, the diffuser geometries (1) to (12) of table I are represented on a plot of area ratio A_e/A_T against length to diameter ratio L_d/D_e in figure 8. The flow of the geometries is indicated as either separated or unseparated. A separation boundary was estimated by using the minimum values of C_f from figures 6 and 7 as an indication of the proximity of separation. Because of the uncertainty in determining the exact location of this separation boundary, it is shown as a separation band with the upper separation line shown dotted. Since the slope of minimum C_f against area ratio is nearly linear and steep, the estimated separation boundaries are reasonably located even at large L_d/D_e. The flow in geometries falling above this boundary would be expected to separate while the flow in those falling below the boundary would remain attached.

For a given area ratio A_e/A_T the designers should choose the minimum length diffuser along the separation boundary in order to increase the efficiency of the diffuser and to minimize weight and skin friction losses. If larger area ratios above the separation boundary than indicated in figure 8 are required for a given application, some means of boundary-layer control will be necessary.

Model and full-scale comparisons. - A comparison of boundary-layer parameters of some of the previous geometries at model (D_e = 30.5 cm (1 ft)) and full-scale (D_e = 183 cm (6 ft)) sizes is presented in figure 9. Because of the expense of full-scale testing, it is very important that the designer has some guidelines to extrapolate from model to full scale. The surface Mach number distributions for both sizes are the same as shown in figures 6(a) and 7(a) since potential flow calculations are independent of scale. Similar general trends in the boundary-layer parameters are evident for both model and full scale. However, the local Reynolds number at full scale is six times the local Reynolds number at model size. This results in less tendency to separate for the full-scale sizes because the minimum value of skin friction coefficient is further away from zero than at the model size (fig. 9(a)). For example, the flow of diffuser 3 is separated at model size but attached at full scale. The nondimensional displacement thicknesses are also thinner at full scale (fig. 9(b)). The results of full-scale calculations for diffusers 1 to 12 are summarized in figure 10. As was done for model size, the minimum value of C_f and its proximity to separation were used to estimate the location of the separation boundary.

Low-speed conditions at angle of attack. - A series of calculations were carried out at model size to show the effect of an incidence angle α of 40°. The surface Mach number distribution and boundary-layer parameters for the windward side of the diffuser are presented in figure 11(a). Higher Mach numbers and larger Mach number gradients occur on the diffuser surface when the inlet is at an incidence angle. These high Mach numbers may give local shocks. However, the effects of shocks were not considered in the analysis. The skin friction coefficient (fig. 11(b)) indicates separation of the flow in all the diffuser geometries except 4 and 9 which have a diffuser area ratio A_e/A_T of 1.2. The separation results for all the diffuser geometries and the estimated separation boundary for the 40° incidence angle is shown in figure 12.

Summary of low-speed conditions. - A summary plot of the estimated boundaries for low-speed conditions is shown in figure 13. All three separation boundaries increase with L_d/D_e. The effect of increasing the scale is to move the separation boundary upward. This requires diffusers at a given area ratio to operate at shorter lengths with attached flows. The effect of increasing the incidence angle is to lower the separation boundary. For a diffuser operating with an incidence of 40°, the diffuser area ratio A_e/A_T should be below 1.5 for unseparated flow. At zero incidence angle the diffuser area ratio can be as high as 1.7 and the flow can be unseparated. Equivalent conical half angle lines of 4°, 5°, and 6° are shown on the plot. The 6° line is often used as a guideline for unseparated flow of diffusers (ref. 1). This line falls along the separation boundary for scale model at $\alpha = 0^\circ$ for L_d/D_e ranging from 0.5 to 0.85. For L_d/D_e greater than 0.85, the 6° conical line falls above the separation boundary predicted by the present analysis. As the length to diameter ratio L_d/D_e increases the separation boundaries cross over to lower equivalent conical half angles.

Cruise conditions. - As a supplement to the preceding low-speed predictions, additional calculations were obtained with a free-stream Mach number M_∞ of 0.75. The surface Mach number distributions and boundary-layer parameters are presented in figure 14 for model size at an incidence angle of 0°. The Mach number gradients are not as severe along the surface as were obtained in the low-speed cases (figs. 6(a) and 7(a)). Of the geometries investigated, diffuser 12 is the only geometry for which separated flow was obtained at cruise conditions compared with four of the designs with separated flows at low speeds. One may conclude that the cruise condition is less severe than the low-speed condition. Thus, the separation boundary will be shifted to greater diffuser area ratios as the free-stream velocity is increased.

Effect of Diffuser Contour

The previous results were obtained using a cubic contour with the deflection point located at 50 percent of the diffuser length. Additional contours were generated with inflection points located at 25 and 75 percent of the diffuser length (fig. 4). The effect of the diffuser contours is presented in figure 15 for diffusers 10, 13, and 14 at an incidence angle of 0° and in figure 16 for diffusers 4, 15, and 16 at an incidence angle of 40°. Conservative diffuser geometries were chosen at a 40° incidence angle since all the geometries of figure 15 separated at a 40° incidence angle. The surface Mach number distribution shows little effect of diffuser contour near the entrance or exit. However, significant variation is noted in the central portion of the diffuser.

The diffuser geometries with inflection points at 25 and 50 percent of length remain attached. However, at incidence angles of 0° (fig. 15) and 40° (fig. 16), the flow of the diffuser with the inflection point at 75 percent of length separated at approximately its inflection point. Examination of figures 15(b) and 16(b) shows little differences in the minimum values of skin friction coefficient for the diffusers with the inflection point at 25 and 50 percent of length. For some overall diffusion it is usually better to diffuse more rapidly in the first portion of the diffuser. Thus, one may conclude that separation is less likely to occur if the inflection point is moved to or ahead of the midpoint of the diffuser.

Effect of Lip Geometry

The effect of lip geometry on diffuser Mach number distributions and boundary-layer parameters is presented in figure 17. The lip geometry was varied by considering internal lip contraction ratios of 1.26, 1.35, and 1.42. The surface Mach number distributions indicate that the 1.26 contraction lip has the highest peak Mach number and Mach number gradient near the diffuser entrance. The Mach number distribution in the diffuser is affected moderately but only near the entrance. The boundary-layer parameters indicate that the flow of the diffuser with the 1.26 contraction ratio lip separated. However, there are small differences in the minimum skin friction coefficient for lip contraction ratios of 1.35 and 1.42. The general trend is that the larger the contraction ratio the greater the resistance of the diffuser to flow separation.

Effect of Throat Mach Number

The previous results were obtained using a throat Mach number of 0.6. For a given diffuser geometry the effects of throat Mach number ranging from 0.5 to 0.8 are presented in figure 18. The Mach number level shifts upward with an increase of throat Mach number and greater overall diffusion, although the curves retain a generally similar shape. The boundary-layer parameters indicate an increased tendency to separate as the throat Mach number is increased. For the diffuser geometry considered in figure 18 ($L_d/D_e = 1.2$, $A_e/A_T = 1.6$), flow separation was obtained at a throat Mach number of 0.8.

The results of this series of calculations are summarized in figure 19 by showing the effect of throat Mach number on the estimated separation boundary. Increasing the throat Mach number shifts the separation boundary downward, thus restricting the range of length to diameter ratio and area ratio for which the flow will remain attached.

SUMMARY OF RESULTS

Theoretical Mach number distributions and boundary-layer parameters were presented for subsonic diffuser geometries with length to exit diameter ratios ranging from 0.4 to 1.6 and exit area to throat area ratios ranging from 1.1 to 2.0. The major portion of the study was done with a cubic contour with the inflection point at the midpoint of the diffuser and with a diffuser entrance Mach number of 0.6 and a free-stream Mach number of 0.12. Calculations were performed at both model (diffuser exit diameter, 30.5 cm) and full-scale (diffuser exit diameter, 183 cm) sizes. Separation limits have been defined by establishing a separation boundary on plots of diffuser area ratio against diffuser length to diameter ratio. The effects of diffuser contour, inlet lip geometry, and throat Mach number on the boundary-layer characteristics are illustrated. The principal results of this study are as follows:

(1) The longer the diffuser length and the smaller the diffuser area ratio, the less likely the flow is to separate. However, there appears to be a maximum value of diffuser area ratio beyond which flow separation will always occur. For small values of diffuser lengths, the 6° equivalent conical half-angle line falls along the separation boundary for scale model at 0°.

(2) The separation boundary will be shifted to greater diffuser area ratios by the following changes in geometry:

- (a) Increasing the diffuser length
- (b) Increasing the size of the diffuser
- (c) Increasing the inlet lip contraction ratio
- (d) Moving the inflection point of the diffuser contour to or ahead of the midpoint of the diffuser

(3) The separation boundary will be shifted to greater diffuser area ratios by the following changes in flow conditions:

- (a) Decreasing the incidence angle
- (b) Increasing the free-stream velocity
- (c) Decreasing the throat Mach number

(4) For a given diffuser area ratio, the designer should choose the minimum length diffuser along the separation boundary in order to increase the efficiency of the diffuser and to minimize weight and skin friction losses.

It is felt that the separation limits set forth in this report will provide useful guidelines for designing separation free inlet diffusers for propulsion systems. However, experimental data are needed to confirm these analytical results.

Lewis Research Center,
National Aeronautics and Space Administration,
Cleveland, Ohio, January 21, 1974,
501-24.

REFERENCES

1. Henry, John R.; Wood, Charles C.; and Wilbur, Stafford W.: Summary of Subsonic-Diffuser Data. NACA RM L56F05, 1956.
2. Reneau, L. R.; Johnston, J. P.; and Kline, S. J.: Performance and Design of Straight, Two-Dimensional Diffusers. Jour. of Basic Eng., Trans. ASME, Series D, vol. 89, no. 1, March 1967, pp. 141-150.
3. Sovran, Gino; and Klomp, Edward D.: Experimentally Determined Optimum Geometries for Rectilinear Diffusers with Rectangular, Conical or Annular Cross-Section. Symposium on the Fluid Mechanics of Internal Flow, G. Sovran ed., Elsevier Publishing Company (Amsterdam), 1962, pp. 270-319.
4. McMillan, O. J.; and Johnston, J. P.: Performance of Low-Aspect-Ratio Diffusers with Fully Developed Turbulent Inlet Flows. Part 1 - Some Experimental Results. Paper 73-FE-12, ASME, July 1973.
5. Runstadler, P. W. Jr.; and Dolan, F. X.: Further Data on the Pressure Recovery Performance of Straight-Channel, Plane-Divergence Diffusers at High Subsonic Mach Numbers. Paper 73-FE-5, ASME, July 1973.
6. Albers, J. A.; and Stockman, N. O.: Calculation Procedures for Potential and Viscous Flow Solutions for Engine Inlets. Paper 74-GT-3, ASME, 1974.
7. Albers, James A.: Theoretical and Experimental Internal Flow Characteristics of a 13.97-Centimeter-Diameter Inlet at STOL Takeoff and Approach Conditions. NASA TN D-7185, 1973.
8. Albers, J. A.: Application of Compressibility Correction to Calculation of Flow in Inlets. Jour. of Aircraft, vol. 10, no. 7, July 1973, pp. 441-442.
9. Albers, James A.: Comparison of Predicted and Measured Low Speed Performance of Two 51-Centimeter-Diameter Inlets at Incidence Angle. NASA TM X-2937, 1973.

10. Albers, James A.; and Miller, Brent A.: Effect of Subsonic Inlet Lip Geometry on Predicted Surface and Flow Mach Number Distributions. NASA TN D-7446, 1973.

11. Herring, H. J.; and Mellor, G. L.: Computer Program for Calculating Laminar and Turbulent Boundary Layer Development in Compressible Flow. NASA CR-2068, 1972.

12. Herring, H. James, and Mellor, George L.: A Method of Calculating Compressible Turbulent Boundary Layers. NASA CR-1144, 1969.

13. Stockman, Norbert O.; and Button, Susan L.: Computer Programs for Calculating Potential Flow in Propulsion System Inlets. NASA TM X-68278, 1973.

14. Hess, J. L.; and Smith, A. M. O.: Calculation of Potential Flow About Arbitrary Bodies. Progress in Aeronautical Sciences. Vol. 8. D. Kuchemann, ad., Pergamon Press, 1967, pp. 1-138.

15. Stockman, Norbert O.: Potential Flow Solutions for Inlets of VTOL Lift Fans and Engines. Analytic Methods in Aircraft Aerodynamics. NASA SP-228, 1970, pp. 659-681.

16. Lieblein, S.; and Stockman, N. O.: Compressibility Correction for Internal Flow Solutions. J. Aircraft, vol. 9, no. 4, Apr. 1972, pp. 312-313.

17. Albers, James A.; and Gregg, John L.: Computer Program for Calculating Laminar, Transitional, and Turbulent Boundary Layers for a Compressible Axisymmetric Flow. NASA TN D-7521, 1974.

18. Schlichting, Herman (J. Kestin trans.): Boundary Layer Theory. Sixth ed., McGraw-Hill Book Co., Inc., 1968, pp. 431-516.

TABLE I. - INLET DIFFUSER GEOMETRIC VARIABLES CONSIDERED

[Diffuser exit diameter for model size, 30.5 cm; diffuser exit diameter for full-scale size, 183 cm.]

Diffuser	Diffuser length to diameter ratio, L_d/D_e	Diffuser area ratio, A_e/A_T	Location of diffuser inflection point, percent of length	Diffuser contour	Internal lip contraction ratio, A_1/A_T	Maximum local wall angle, β, deg	Equivalent conical half angle, $\theta/2$, deg
1	0.4	1.1	50	Cubic	1.35	13.36	3.1
2	.4	1.2				17.02	5.6
3	.6	1.4				15.70	6.7
4	.8	1.2				8.70	2.9
5	.8	1.4				11.91	5.1
6	.8	1.6				14.45	6.8
7	.9	1.4				10.61	4.5
8	.9	1.5				11.76	5.3
9	1.2	1.2				5.83	1.9
10	1.2	1.6				9.75	4.6
11	1.6	1.6				7.34	3.4
12	1.6	2.0				9.36	4.8
13	1.2	1.6	25	Two superellipses		9.75	4.6
14	1.2	1.6	75			9.75	4.6
15	.8	1.2	25			8.70	2.9
16	.8	1.2	75			8.70	2.9
17	1.2	1.6	50	Cubic	1.26	9.75	4.6
18	1.2	1.6	50	Cubic	1.42	9.75	4.6

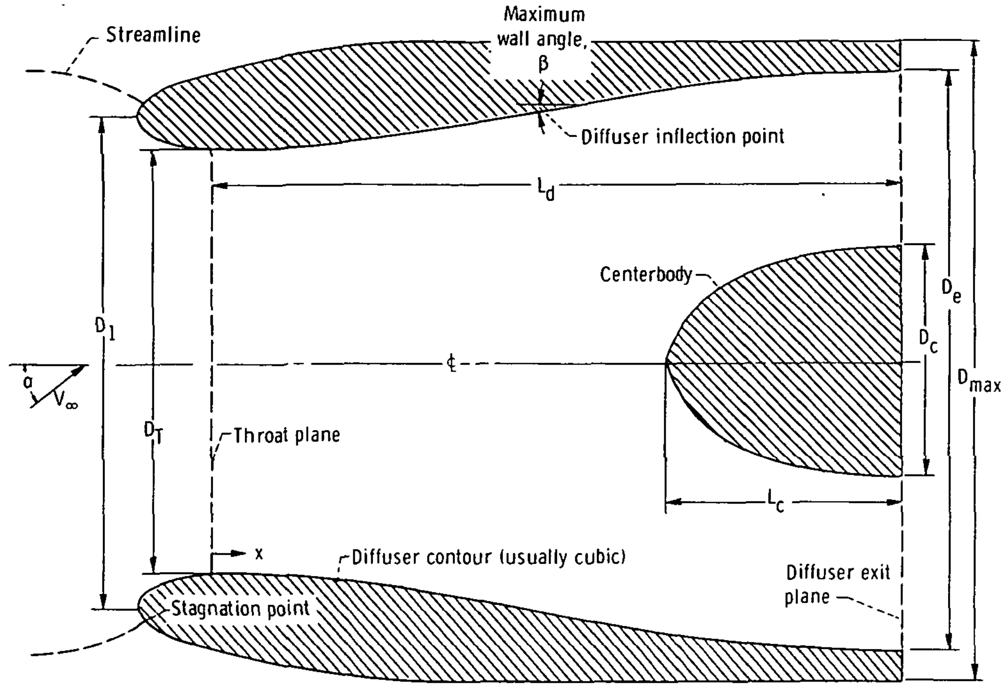

Figure 1. - Illustration of inlet diffuser geometric variables.

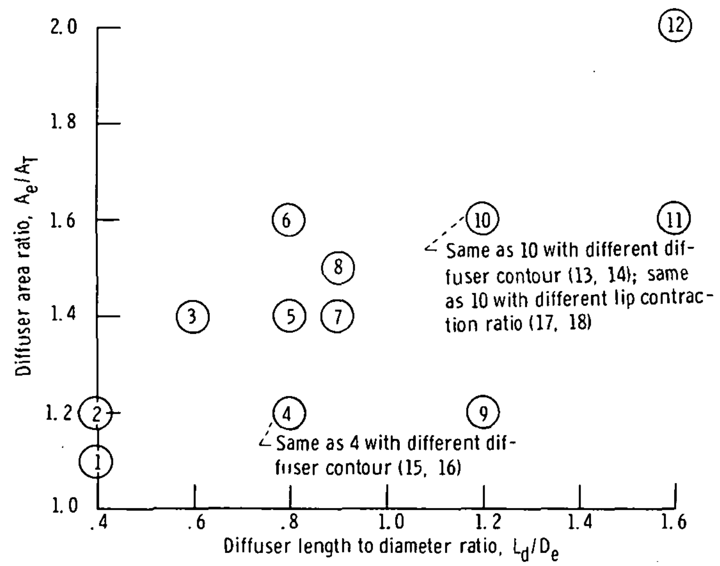

Figure 2. - Diffuser area ratios and diffuser length to diameter ratios considered in this investigation.

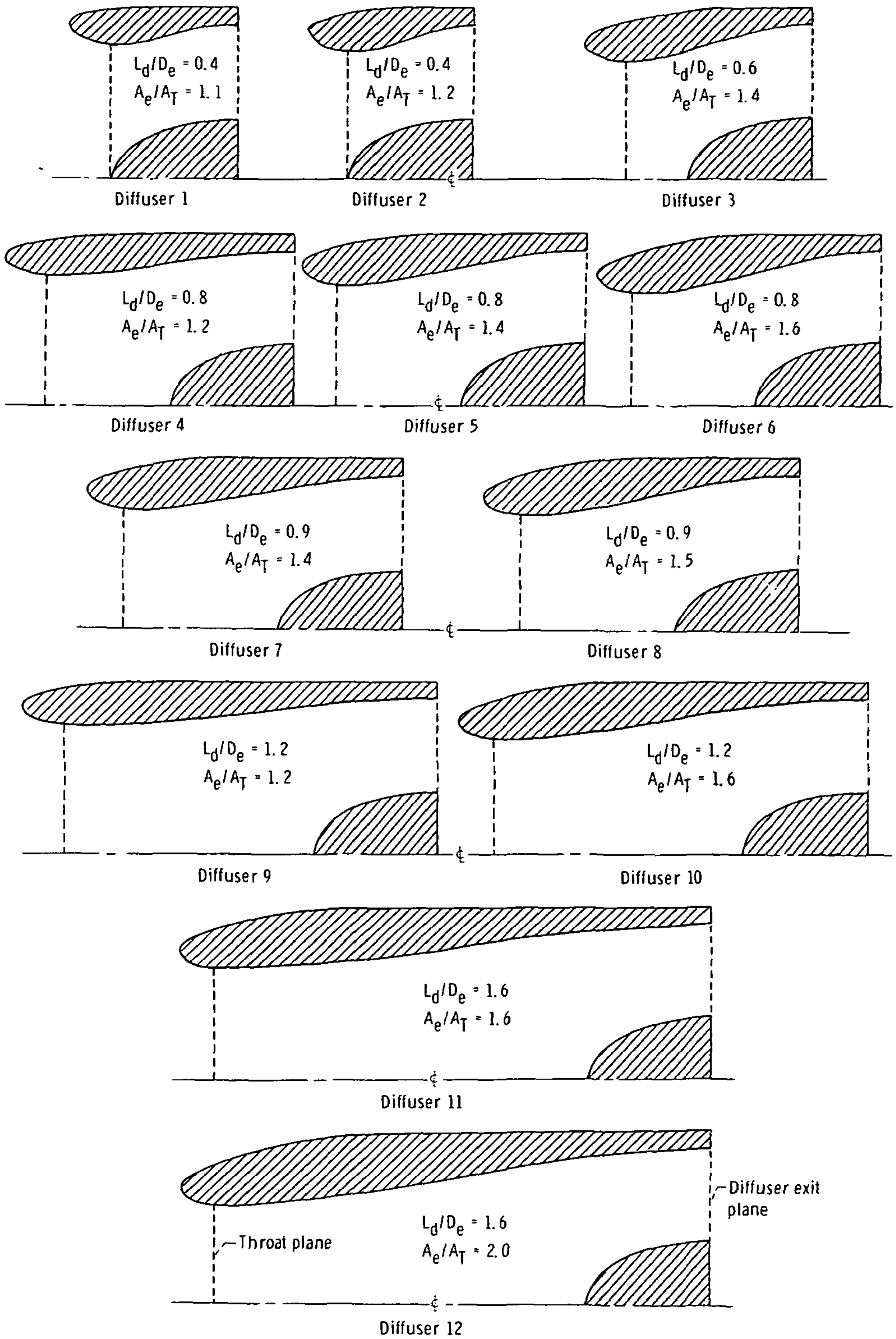

Figure 3. - Illustration of inlet diffuser geometries for various length to diameter ratios (L_d/D_e) and area ratios (A_e/A_T). Diffuser contour, cubic.

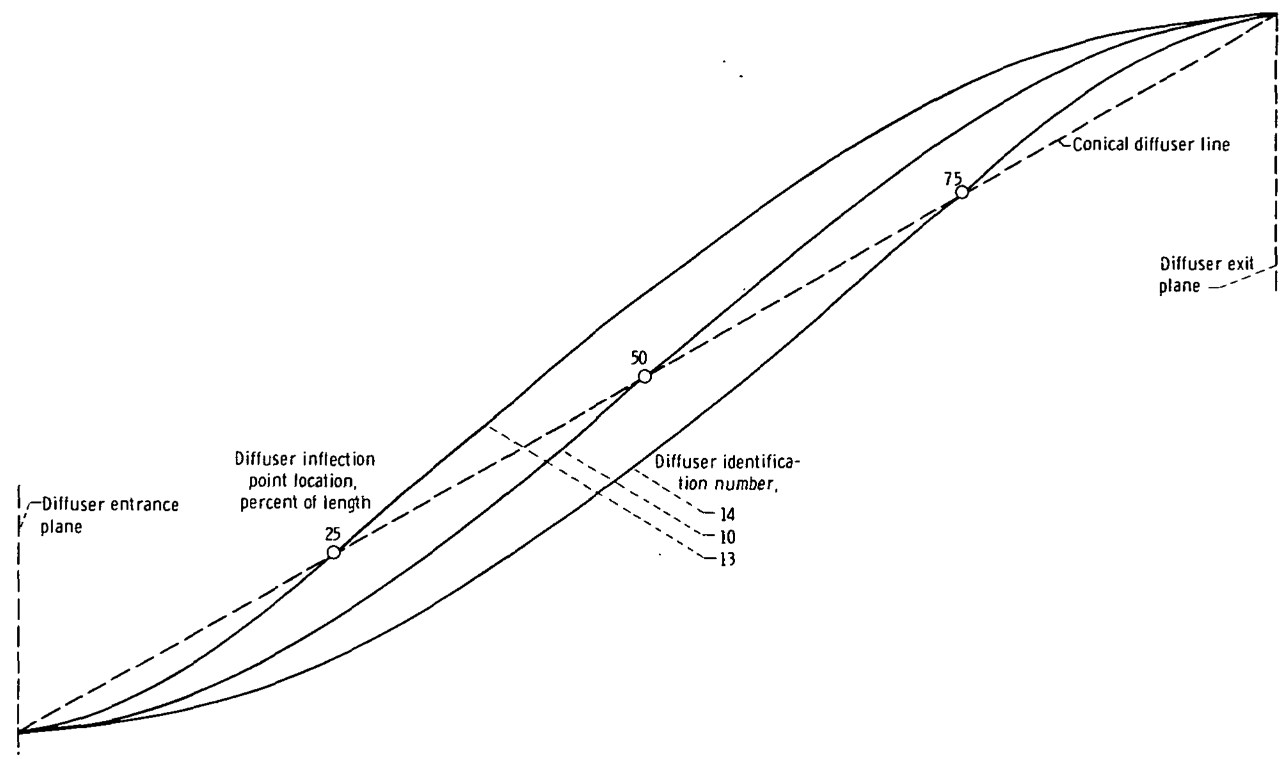

(a) Diffuser length to diameter ratio, L_d/D_e, 1.2; diffuser area ratio, A_e/A_T, 1.6.

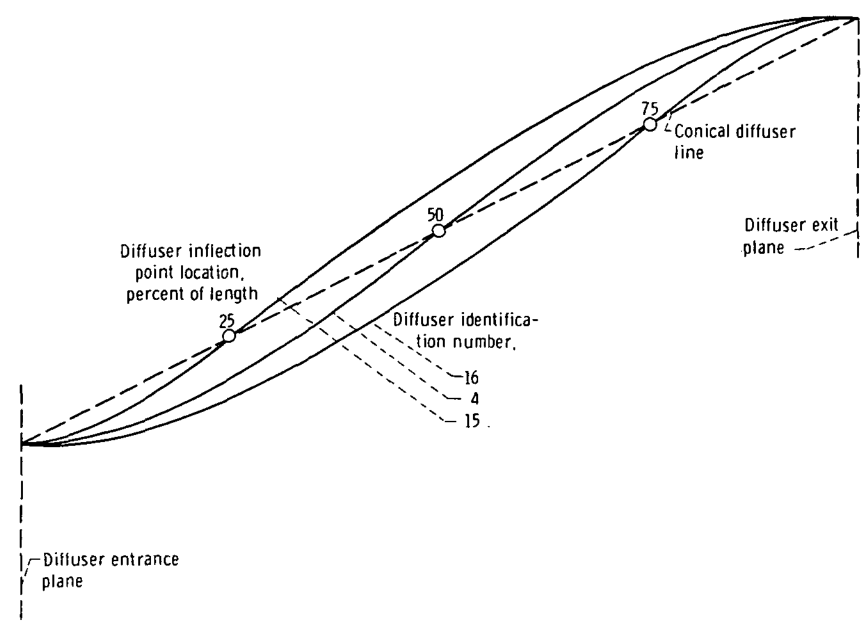

(b) Diffuser length to diameter ratio, L_d/D_e, 0.8; diffuser area ratio, A_e/A_T, 1.2.

Figure 4. - Diffuser contour geometries (expanded vertical scale).

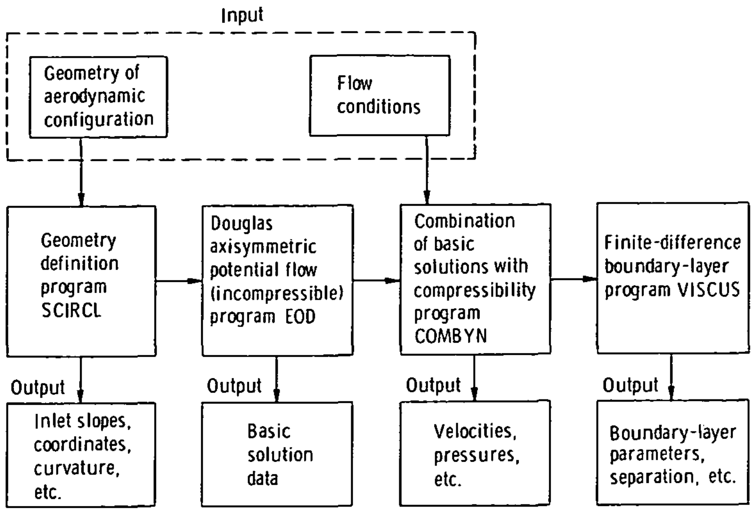

Figure 5. - Schematic of calculation procedure.

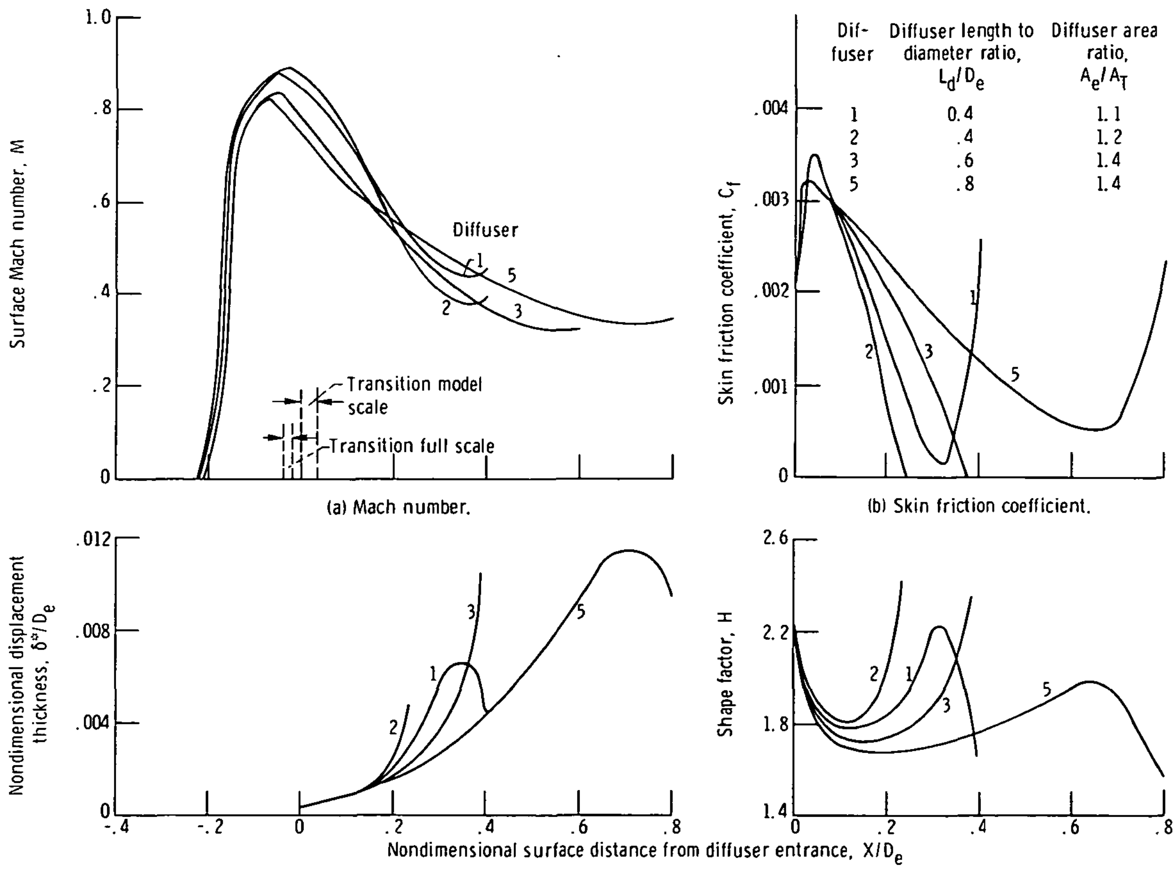

Figure 6. - Effect of diffuser geometry on boundary-layer characteristics for length to diameter ratios L_d/D_e from 0.4 to 0.8. Throat Mach number, M_T, 0.6; free-stream Mach number, M_∞, 0.12; inlet incidence angle, α, 0^0; model size, D_e = 30.5 centimeters; internal lip contraction ratio, A_l/A_T, 1.35.

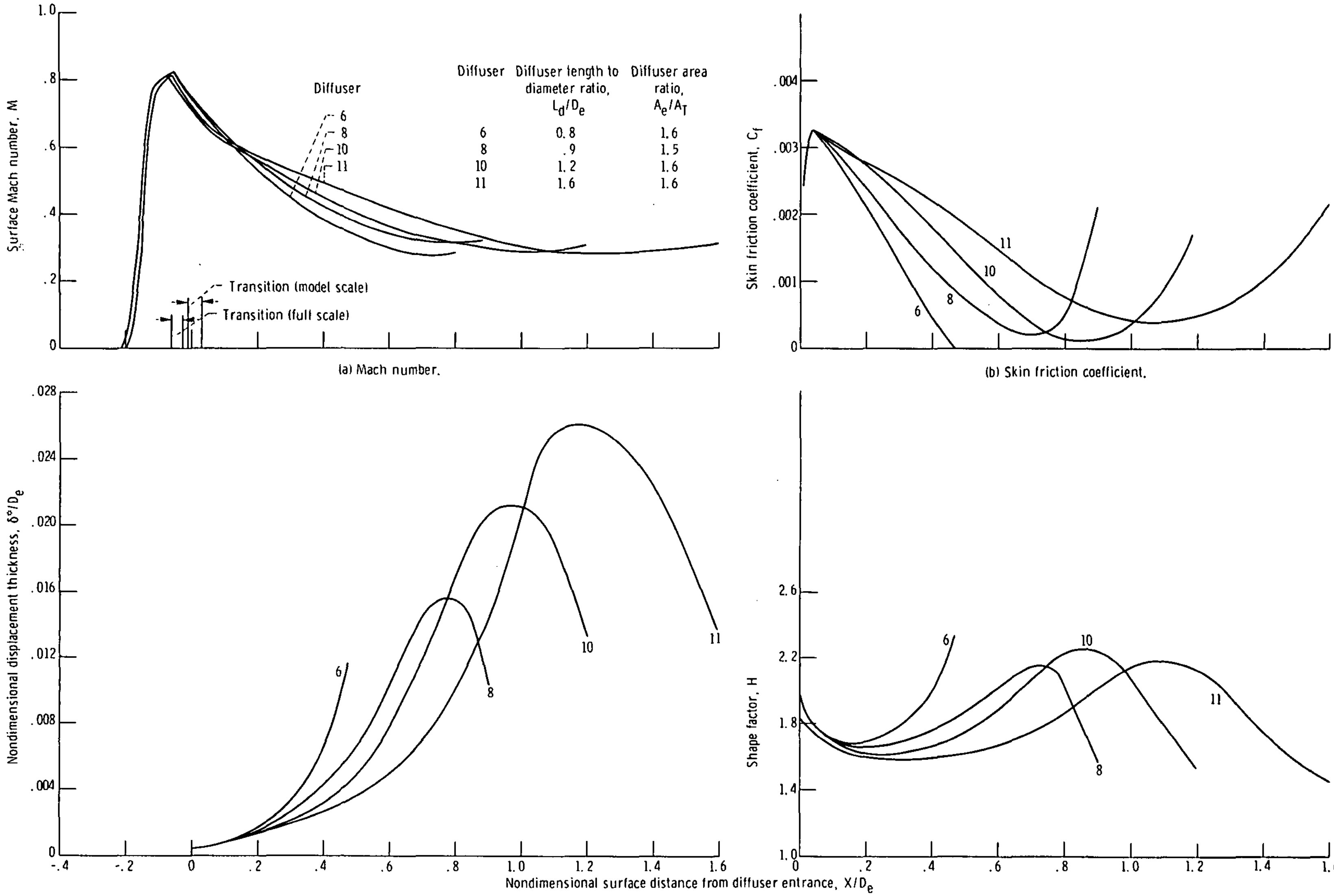

(a) Mach number.

(b) Skin friction coefficient.

(c) Displacement thickness.

(d) Shape factor.

Figure 7. - Effect of diffuser geometry on boundary-layer characteristics for length to diameter ratios L_d/D_e from 0.8 to 1.6. Throat Mach number, M_T, 0.6; free-stream Mach number, M_∞, 0.12; inlet incidence angle, α, 0^0; model size, D_e = 30.5 centimeters; internal lip contraction ratio, A_l/A_T, 1.35.

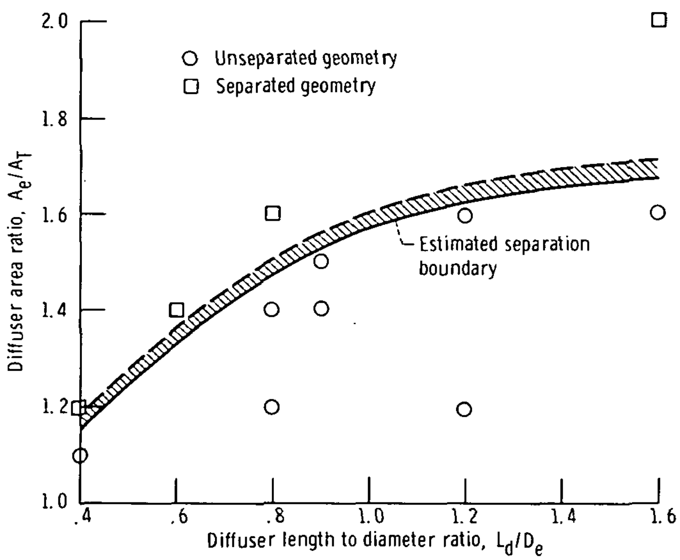

Figure 8. - Separation boundary for diffuser geometries. Free-stream Mach number, M_∞, 0.12; inlet incidence angle, α, 0^0; throat Mach number, M_T, 0.6; model size, D_e = 30.5 centimeters.

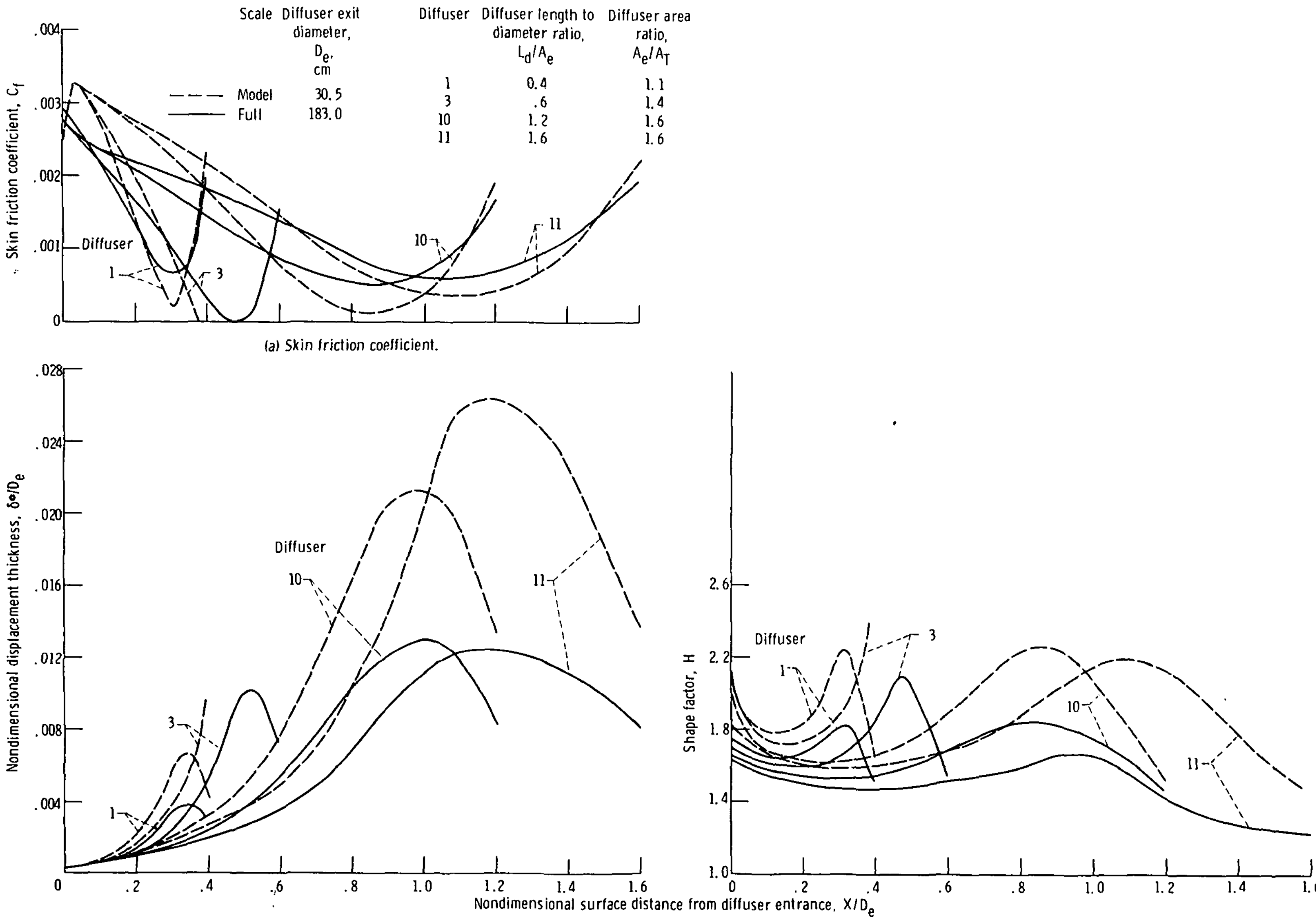

(b) Displacement thickness.

(c) Shape factor.

Figure 9. - Comparison of model and full scale boundary layer characteristics. Throat Mach number, M_T, 0.6; free-stream Mach number, M_∞, 0.12; inlet incidence angle, 0^o; internal lip contraction ratio, A_1/A_T, 1.35.

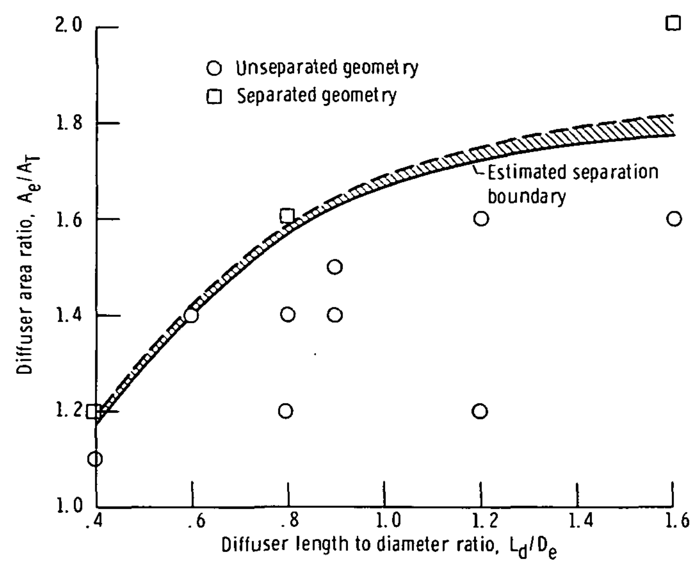

Figure 10. - Separation boundary for diffuser geometries. Throat Mach number, M_T, 0.6; free-stream Mach number, M_∞, 0.12; inlet incidence angle, α, 0^0; full scale, D_e = 183 centimeters.

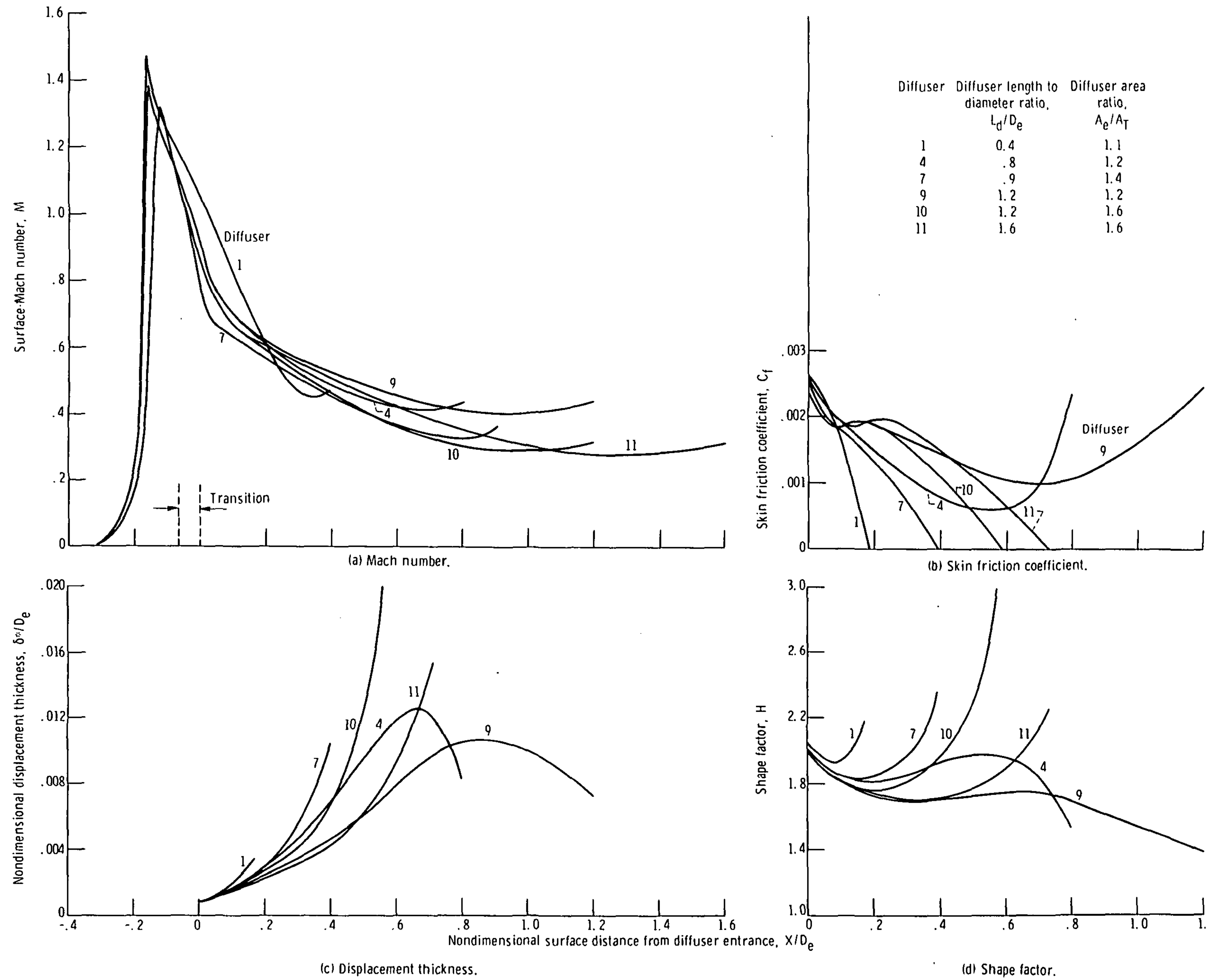

Figure 11. - Effect of diffuser geometry on boundary-layer characteristics for incidence angle α of 40^0. Throat Mach number, M_T, 0.6; free-stream Mach number, M_∞, 0.12; model size, D_e = 30.5 centimeters; internal lip contraction ratio, A_1/A_T, 1.35.

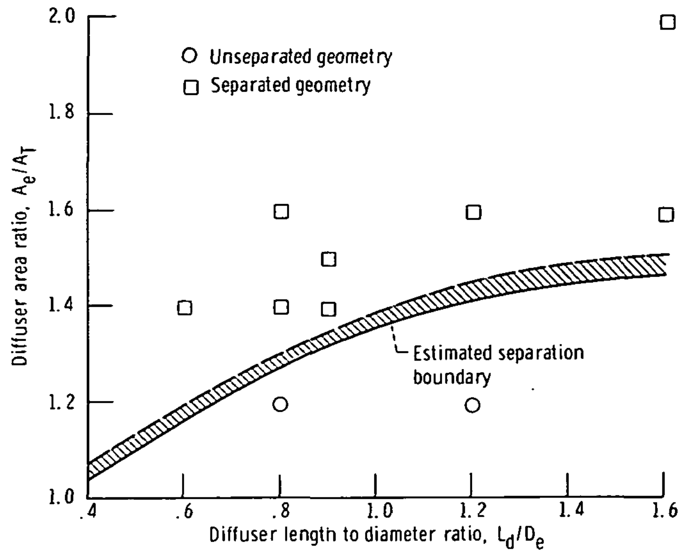

Figure 12. - Separation boundary for diffuser geometries. Throat Mach number, M_T, 0.6; free-stream Mach number, M_∞, 0.12; inlet incidence angle, α, 40^0; model size, D_e = 30.5 centimeters.

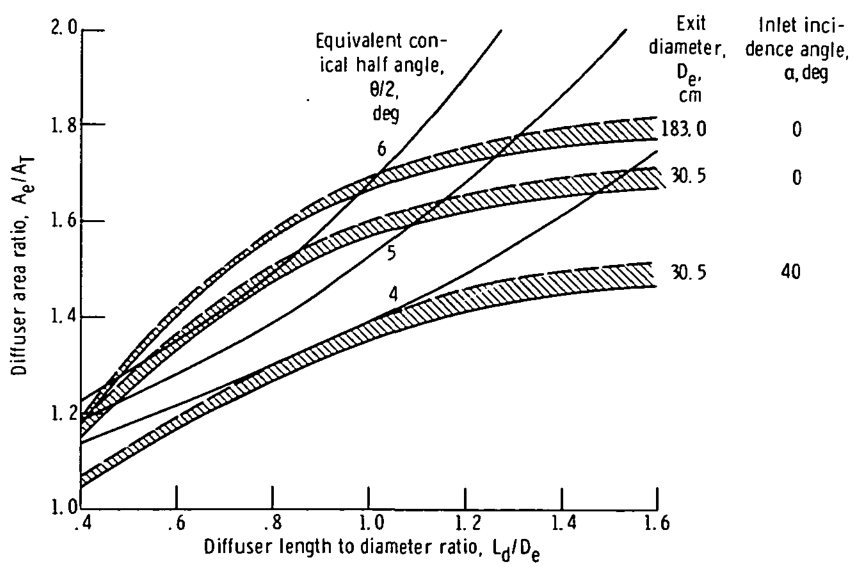

Figure 13. - Summary plot of separation boundaries for low-speed conditions. Throat Mach number, M_T, 0.6; free-stream Mach number, M_∞, 0.12.

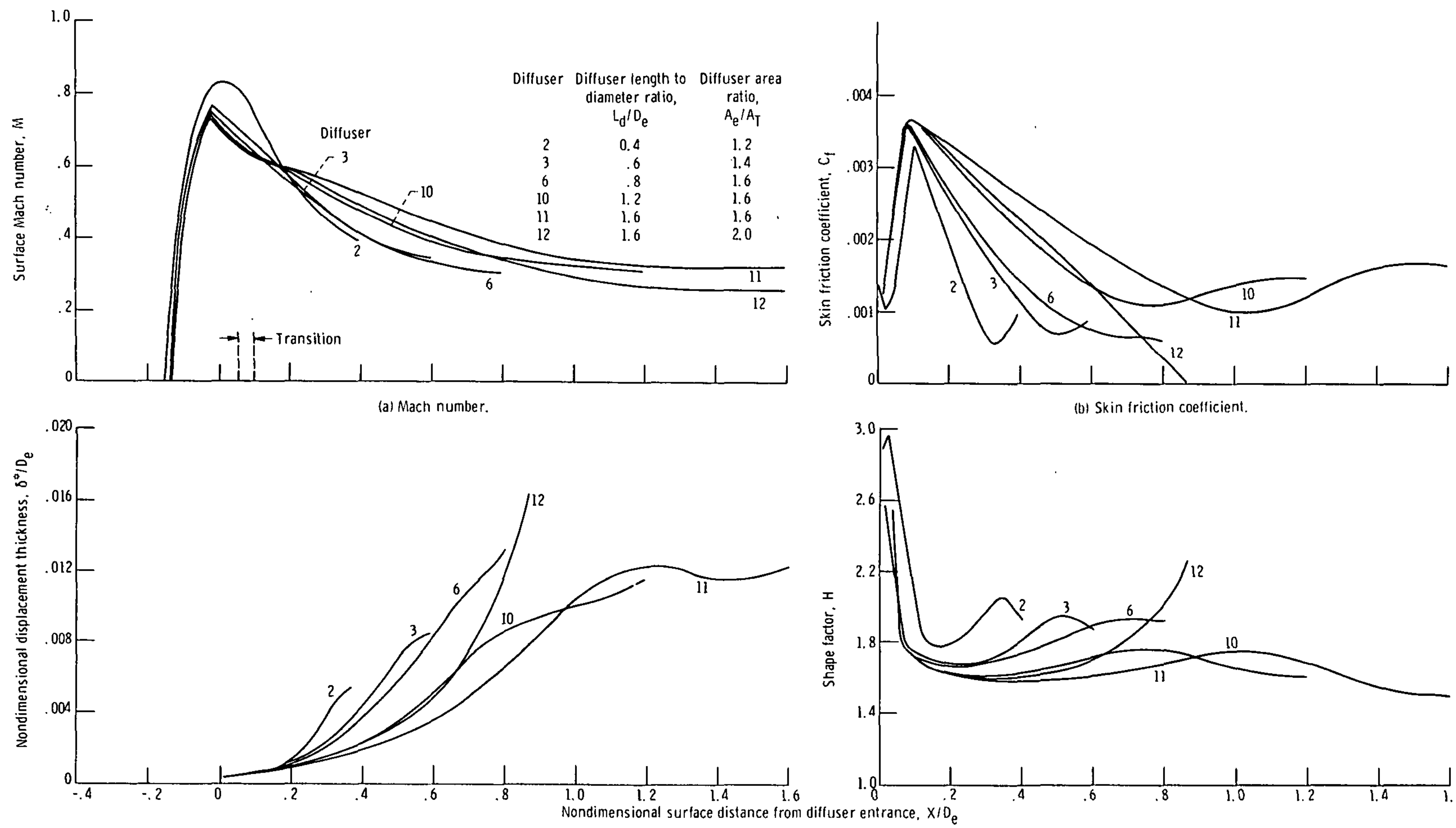

(a) Mach number.

(b) Skin friction coefficient.

(c) Displacement thickness.

(d) Shape factor.

Figure 14. - Effect of diffuser geometry on boundary-layer characteristics for cruise conditions. Throat Mach number, M_T, 0.6; free-stream Mach number, M_∞, 0.75; inlet incidence angle, α, 0^0; model size, D_e = 30.5 centimeters; internal lip contraction ratio, A_1/A_T, 1.35.

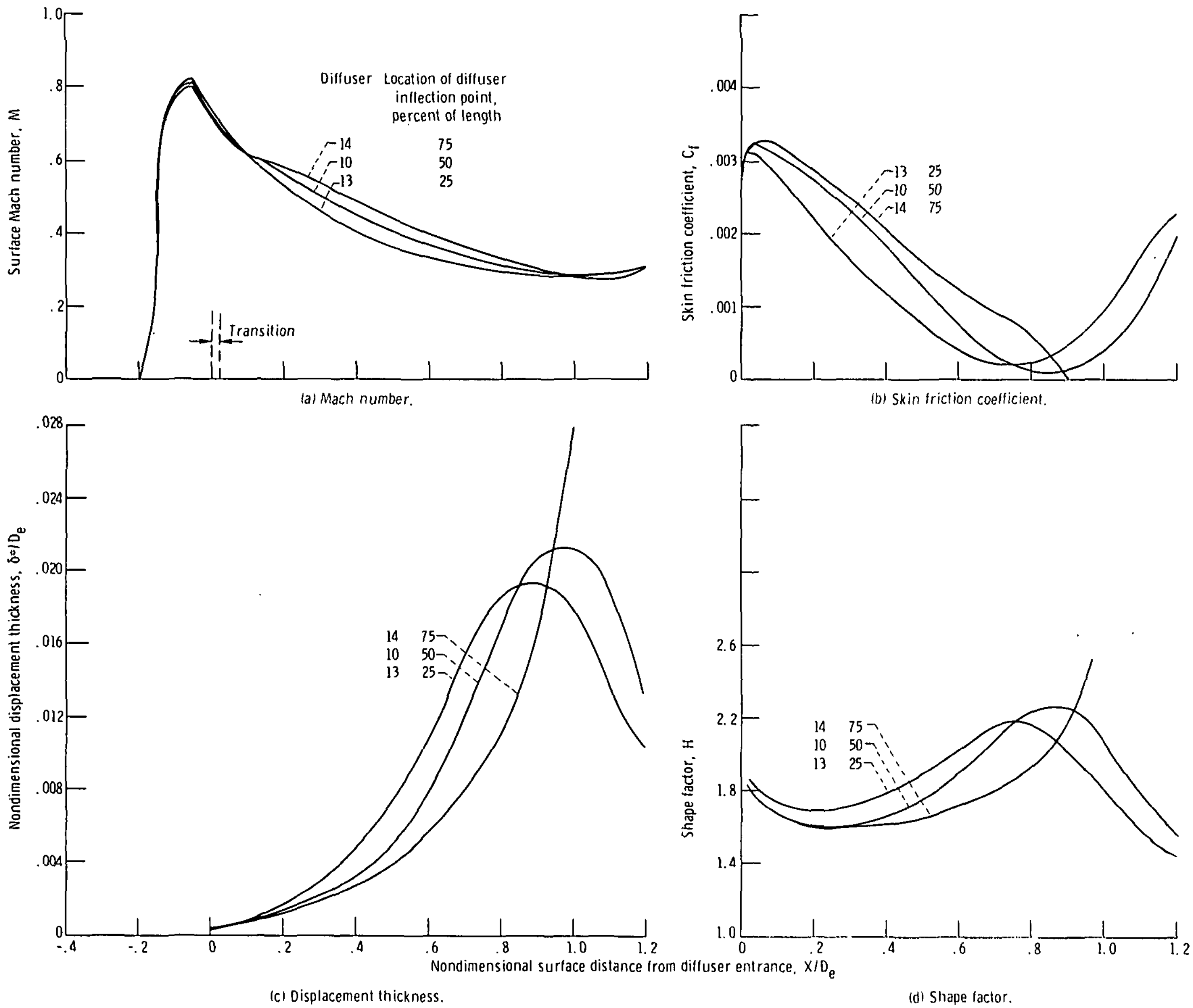

Figure 15. - Effect of diffuser contour on boundary-layer characteristics at inlet incidence angle of 0°. Length to diameter ratio, L_d/D_e, 1.2; *area ratio*, A_e/A_T, 1.6; *throat* Mach number, M_T, 0.6; free-stream Mach number, M_∞, 0.12; model size, D_e = 30.5 centimeters; internal lip contraction, A_1/A_T, 1.35.

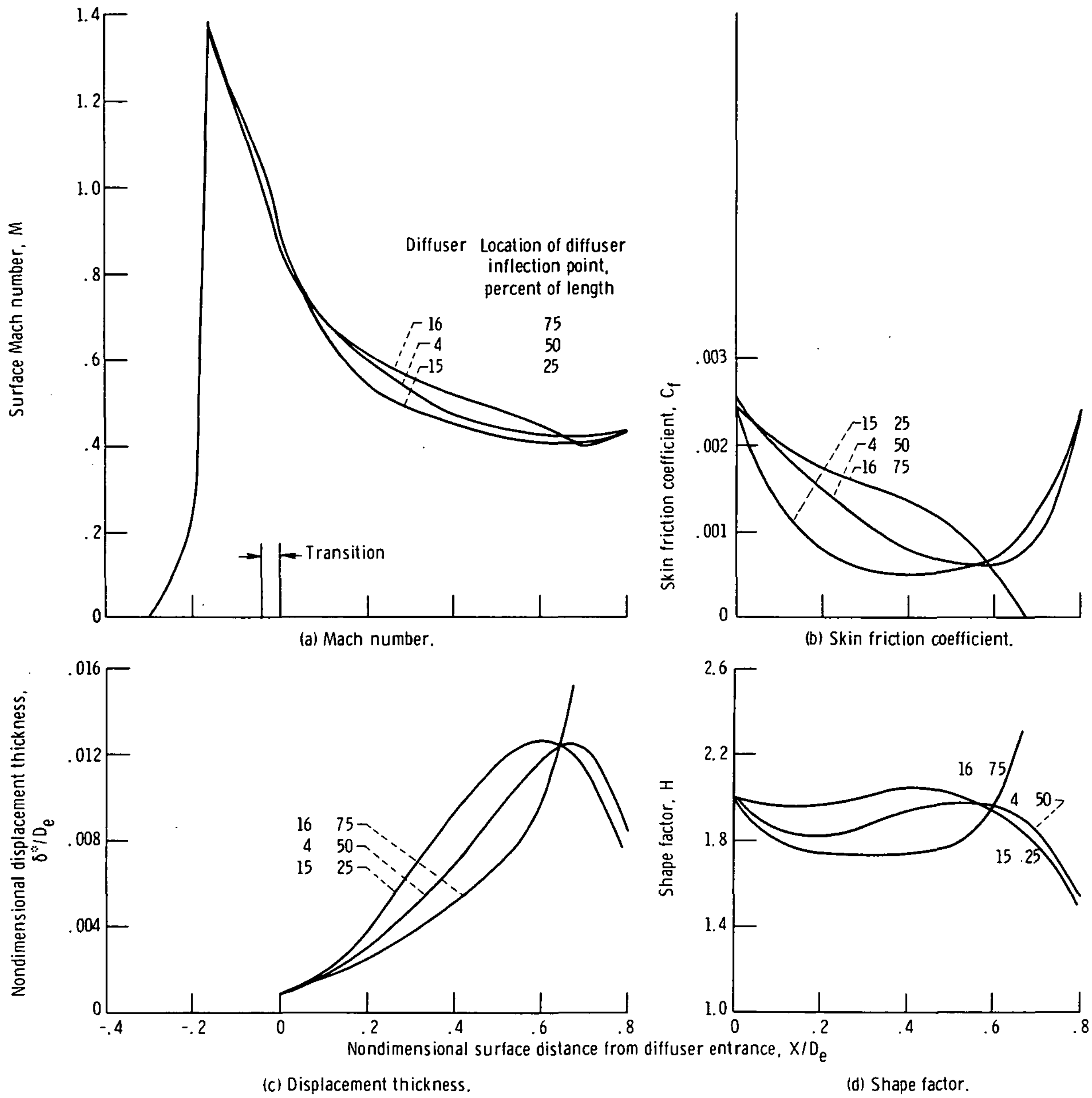

Figure 16. - Effect of diffuser contour on boundary-layer characteristics at inlet incidence angle of 40^0. Length to diameter ratio, L_d/D_e, 0.8; area ratio, A_e/A_T, 1.2; throat Mach number, M_T, 0.6; free-stream Mach number, M_∞, 0.12; model size, D_e = 30.5 centimeters; internal lip contraction ratio, A_l/A_T, 1.35.

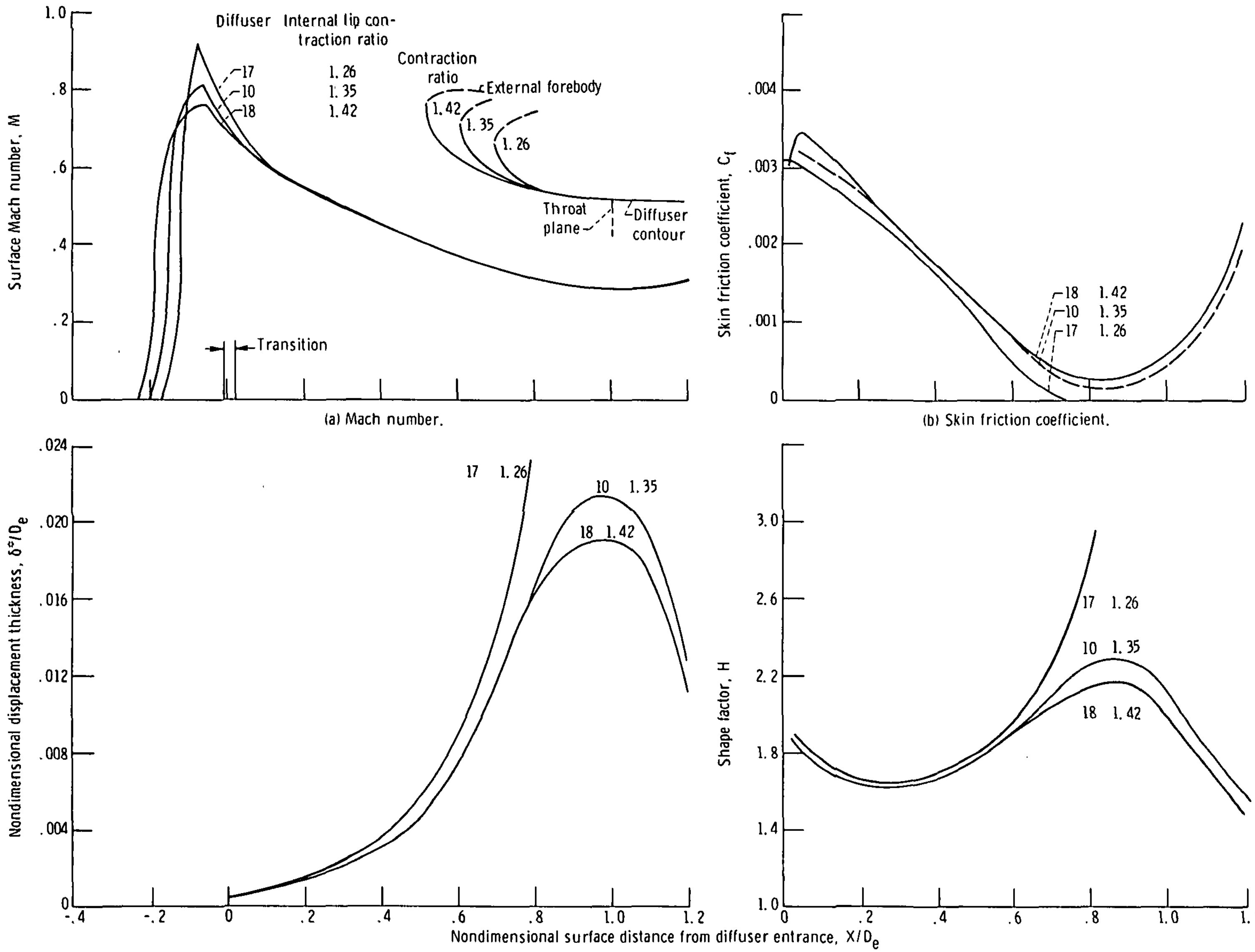

(a) Mach number.

(b) Skin friction coefficient.

(c) Displacement thickness.

(d) Shape factor.

Figure 17. - Effect of inlet lip geometry on diffuser boundary-layer characteristics. Length to diameter ratio, L_d/D_e, 1.2; area ratio, A_e/A_T, 1.6; throat Mach number, M_T, 0.6; free-stream Mach number, M_∞, 0.12; inlet incidence angle, 0^0; model size, D_e = 30.5 centimeters.

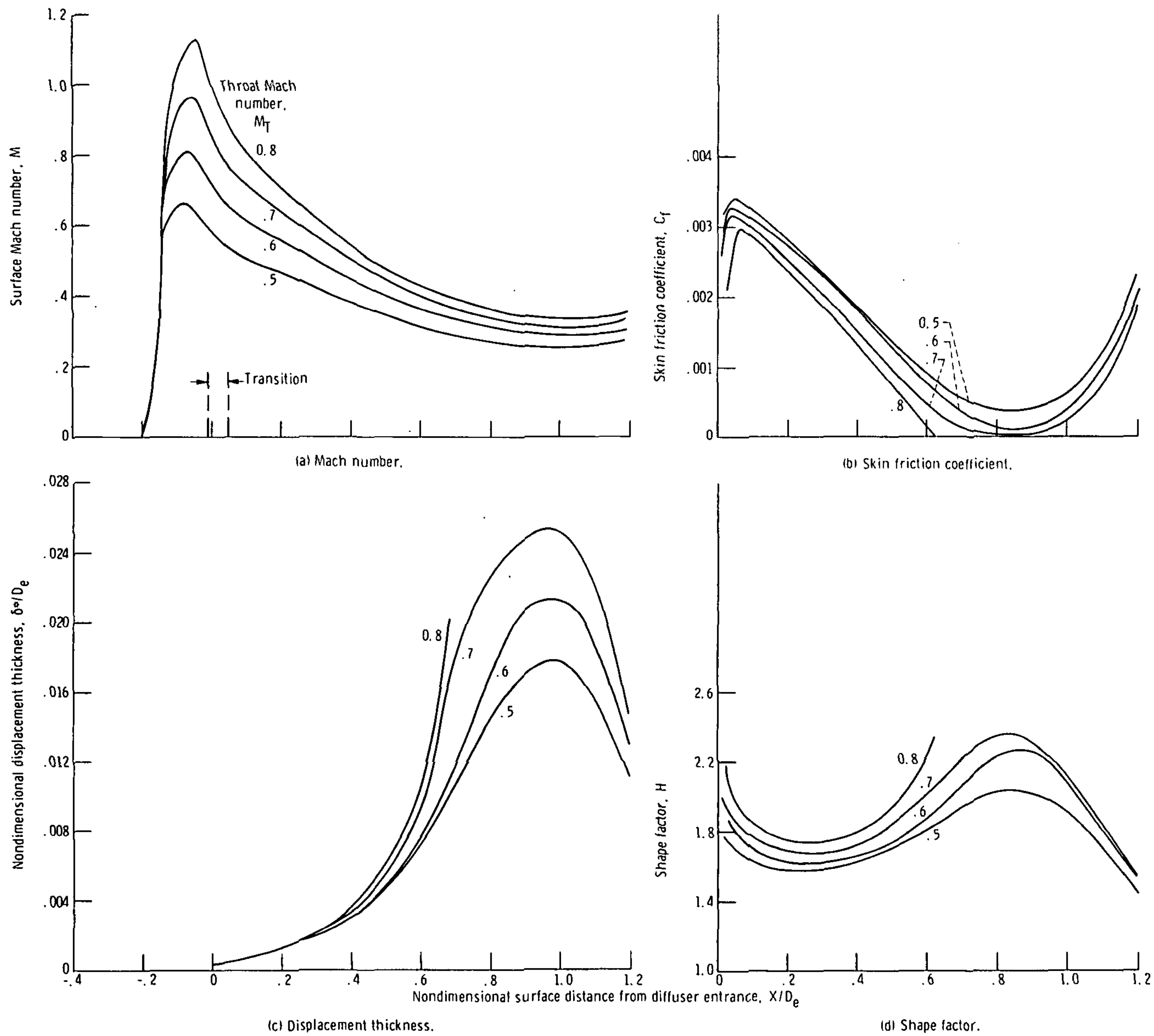

Figure 18. - Effect of throat Mach number, M_T, on diffuser boundary layer characteristics. Length to diameter ratio, L_d/D_e, 1.2; area ratio, A_e/A_T, 1.6; free-stream Mach number, M_∞, 0.12; inlet incidence angle, α, 0^0; model scale, D_e = 30.5 centimeters; diffuser identification number, 10.

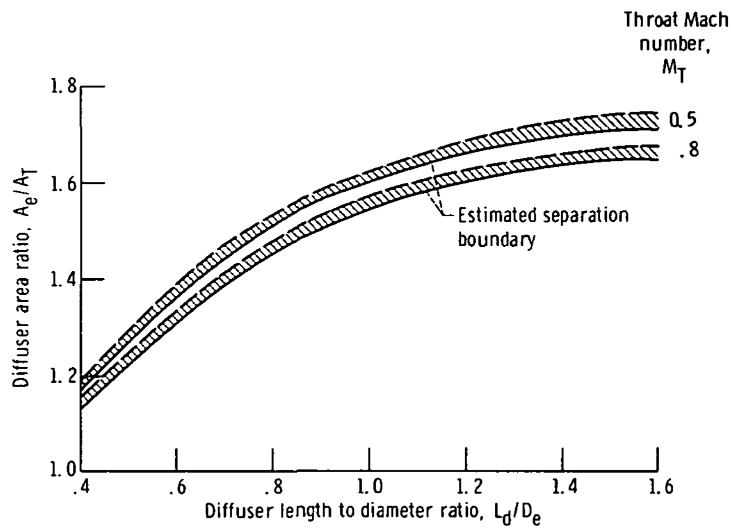

Figure 19. - Separation boundaries for diffuser geometries with various throat Mach numbers M_T. Free-stream Mach number, M_∞, 0.12; inlet incidence angle, 0^0; model size, D_e = 30.5 centimeters.